Copyright 2012, ABRACO
Trabalho apresentado durante o INTERCORR 2012, em Salvador/BA no mês de maio de 2012.
As informações e opiniões contidas neste trabalho são de exclusiva responsabilidade do(s) autor(es).

Macrosegregation and Tertiary Dendrite Arm Spacing Effects on the Corrosion Resistance of a Pb-Sb Alloy for Lead-Acid Battery Components

Emmanuelle S. Freitas[a], Wislei R. Osório[a, b], Leandro C. Peixoto[a], José E. Spinelli[c], Amauri Garcia[a]

Abstract

The aim of this study is to evaluate both the solute (Sb) macrosegregation and tertiary dendrite arm spacing on the corrosion behaviour of a Pb-Sb casting alloy. In this sense, a water-cooled unidirectional solidification system was used to obtain alloy samples having different dendritic patterns. The macrosegregation profile was measured along the casting length. Electrochemical impedance spectroscopy and potentiodynamic polarization curves were used to analyze the corrosion resistance in a 0.5M H_2SO_4 solution at 25ºC. It was found that the tertiary dendritic arms associated with the antimony segregation have an important role on the resulting corrosion response. It is shown that the sample with a well defined tertiary dendritic array provide a more homogeneously distributed interdendritic eutectic mixture exhibiting better corrosion protection. An "enveloping" effect of the Sb-rich lamellae on the Pb-rich phase is more efficient for finer spacing arrays, which is intimately correlated with a more extensive distribution of the eutectic mixture, and thus contributing to the protection of the Pb-rich matrix against corrosion.

Keywords: Lead-acid battery components, Pb-Sb alloys, Corrosion resistance

Introduction

It is well-known that Pb-Sb alloys are commonly used in the production of positive and negative grids, connectors and other components of both VRLA – valve-regulated lead acid and SLI – starting, lighting and ignition batteries (1-20). It is also known that the antimony content of a Pb-Sb electrode affects the mechanical properties, the microstructure, the electrochemical behaviour of active materials and corrosion layers on the electrode (1-3). The cellular and dendritic arm spacings are important microstructural parameters affecting the segregation and mechanical properties. In particular, the scale of cellular and secondary dendritic spacings was shown to strongly influence the overall surface corrosion resistance of binary lead-base alloys. (4-5)

In a recent article, it was shown that a coarser cellular structure tends to yield higher corrosion resistance than finer cellular structures for a dilute Pb-0.85 wt.% Sb alloy (4). Such tendency was associated with the reduction of cellular boundaries when compared with finer cells, since the boundary has proved to be more susceptible to the corrosion action. It is known that antimony, which is segregated toward the cell boundaries and interdendritic regions during solidification of Pb-Sb alloys, has an important role on the corrosion behavior (4-6). Previous studies (4-5) evidenced that coarse cellular samples were associated with better corrosion

[a] Department of Materials Engineering, University of Campinas- UNICAMP, PO Box 6122, 13083–970 Campinas- SP, Brazil
[b] School of Applied Sciences -FCA, University of Campinas- UNICAMP, Campus Limeira, 1300, Pedro Zaccaria St. , Jd. Sta Luiza, 13484-350 Limeira- SP, Brazil
[c] Department of Materials Engineering, Federal University of São Carlos –UFSCar, 13565-905 São Carlos- SP, Brazil

resistance than fine cellular samples when considering experimental studies with Pb-base alloys subjected to corrosion tests in a sulfuric acid (H_2SO_4) solution. In another recent article (7), it was found that the experimental current density increased with the increase in both the Sb content and dendritic spacing, when the dendritic morphological arrays of Pb-2.2 and 6.6 wt.% Sb alloys were compared. It was concluded that independently of the micromorphological array, the Pb-2.2 wt.% Sb alloy sample has better corrosion resistance than both Pb-1 and 6.6 wt.% Sb alloys. (7)

The aim of this study was to examine the effect of both the Sb macrosegregation and the presence of tertiary dendrite arms of a Pb-Sb alloy on the resultant electrochemical corrosion behavior. For this purpose, a Pb-3.5 wt.% Sb alloy and a water cooled unidirectional solidification system were used.

Methodology

Pb-Sb alloy sample was prepared from commercially pure (c.p.) metals: Pb (99.97 wt.%) and Sb (99.99 wt.%). The mean impurities detected were: Fe (0.12 wt.%), Si (0.05 wt.%), Cu (0.015 wt.%), besides other elements with concentration less than 50 ppm.

A water-cooled unidirectional solidification system was used in the experiments. The solidification set-up was designed in such way that the heat was extracted only through the water-cooled bottom, promoting vertical upward directional solidification. More details concerning the directional casting assembly were previously reported. (8-9)

In order to establish correlations between the corrosion resistance and the microstructural pattern, electrochemical impedance spectroscopy (EIS) and polarization tests were carried-out on samples collected at different positions along the casting length. The EIS tests were conducted in a stagnant and naturally aerated 500 cm^3 of 0.5 M H_2SO_4 solution (pH ±0.86) at 25^oC. Electrochemical corrosion tests were performed in a 1 cm^2 circular area of ground (600 and 1200 grit SiC finish) alloy samples. Electrochemical impedance spectroscopy (EIS) measurements began after an initial delay of 15 minutes for the samples to reach a steady-state condition. A potentiostat coupled to a frequency analyzer system, a glass corrosion cell kit with a platinum counter-electrode and a saturated calomel reference electrode (SCE) were used to perform the EIS tests. The potential amplitude was set to 10 mV at open-circuit, peak-to-peak (AC signal), with 5 points per decade and the frequency range was set from 100 mHz to 100 kHz.

Potentiodynamic measurements were conducted by stepping the potential at a scan rate of 0.1667 mV s^{-1} from -0.75 V (SCE) to -0.35 V (SCE) at open-circuit. Duplicate tests for EIS and potentiodynamic polarization curves were carried out. In order to supply quantitative support for discussions of these experimental EIS results, an appropriate model (ZView version 2.1b) for equivalent circuit quantification has also been used.

Results and discussion

Macrostructure, microstructure and cooling rate

The macrostructure of the resulting directionally solidified Pb-3.5wt.%Sb alloy casting is shown in Fig. 1(a). Columnar grains prevailed along the entire casting length, as previously

obtained in other similar experiments using Pb-base alloys (4-5). The positions in the casting from where the samples for microstructure characterisation and corrosion tests were extracted are also indicated in Fig. 1(a). The experimental Sb macrosegregation profile along the casting length is shown in Fig 1(b).

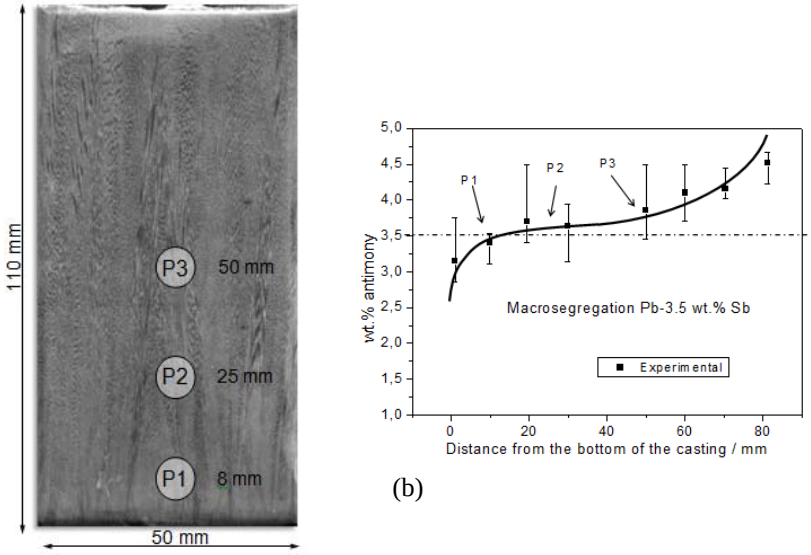

Figure 1 - (a) Macrostructure of a Pb-3.5wt.%Sb alloy casting; P1, P2 and P3 are the positions in casting from where the samples for microstructure characterization and corrosion tests were extracted, (b) Macrosegregation profile along the casting length.

The experimental evolution of the dendrite arm spacings (both primary, λ_1, and tertiary, λ_3) as a function of the resulting cooling rate is shown in Fig. 2. It can be seen that the tertiary dendrite spacing is about 3.7 times lower than the primary dendrite spacing for the range of cooling rates experimentally examined.

A λ_1/λ_3 ratio of about 5 has been reported for Al-Cu alloys unidirectionally solidified. It has also been reported that the tertiary array has a growth character which is very similar to that of cells and primary dendrite arms. (10)

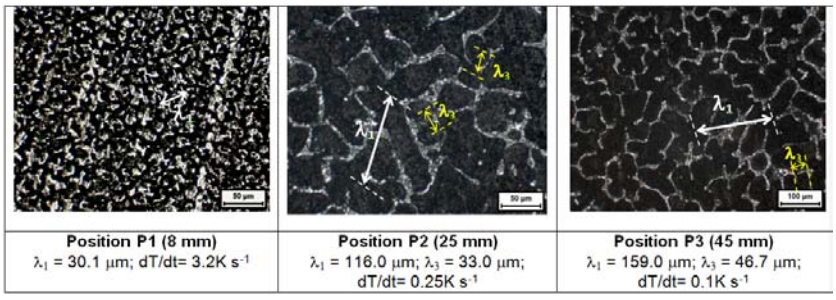

Figure 2 - Typical transverse microstructures along the Pb-3.5wt%Sb alloy casting length and evolution of primary and tertiary dendritic arm spacings with the cooling rate.

It seems that the Sb content associated with the local solidification cooling rate affect the development of dendritic tertiary arms. Higher cooling rates associated with lower Sb content (lower than 3.5 wt.% Sb) which are typical of initial positions in the casting (up to 25 mm

from the bottom of the casting) provide a microstructural dendritic array which is characterized by primary and secondary dendrite arms.

The typical microstructures observed on transverse sections of the Pb-3.5 wt.% Sb alloy casting are also shown in Fig. 2. The as-cast microstructure consists of a dendritic Pb-rich matrix (α-phase: solid solution of Sb in Pb) with a lamellar eutectic mixture in the interdendritic regions constituted of α, and a Sb-rich β-phase (solid solution of Pb in Sb).

EIS measurements and equivalent circuit:
a) Equivalent circuit and Nyquist diagrams

The Fig. 3 depicts Nyquist plots representing Z (Imaginary) and Z (Real), simulated and experimental results in Nyquist plots of all examined Pb-3.5wt.%Sb alloy samples. All Nyquist plots are characterized by a capacitive arc at high frequencies (between 10^5 Hz and 2 Hz). It can also be seen that the Nyquist plot corresponding to the position P3 has a diameter of the capacitive arc which is higher than those corresponding to the samples of the two other positions examined (i.e. P2 and P1). It can also be observed that the Nyquist plot for P3 is the only characterized by a capacitive arc followed by a trend to a slope of about 45^o from 0.25 to 0.01 Hz, which can indicate that an oxide film has formed and is thus contributing to better electrochemical behaviour.

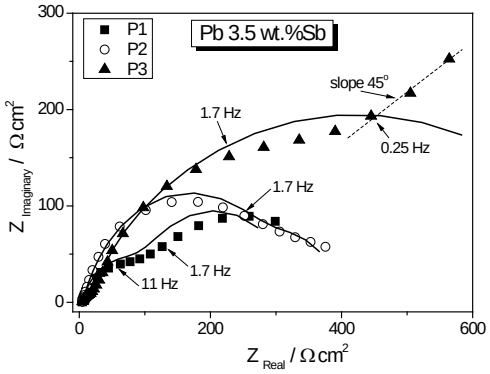

Figure 3 - Experimental and simulated Nyquist results data for the Pb 3.5wt.% Sb alloy samples in a 0.5M H2SO4 solution at 25 °C.

These experimental impedance parameters provide indications that the sample corresponding to the position P3 seems to be correlated with the best electrochemical behaviour when compared to the other samples examined. It seems that the tertiary dendritic arm spacing (λ_3) has an important effect on the resulting corrosion resistance. At position P2 the tertiary arms initiate their development from the secondary branches differently of position P1 where the microstructure has no tertiary dendrite arms, as shown in Fig. 2. Besides, it can also be observed a slightly higher Sb content at P2 (Fig. 1) when compared with P1. When comparing the resulting microstructural arrays of positions P3 and P2, it can be seen that the sample of position P3 has tertiary spacings (of about 50 μm) which are coarser than those observed at P2 (λ_3 of about 25 μm) but the continuity of the tertiary arms along the interdendritic region permits the eutectic mixture to be more homogeneously distributed.

Fig. 4 shows the proposed equivalent circuit used to fit the experimental data. The impedance parameters obtained by the ZView® software, are shown in Table 1. The fitting quality was evaluated by chi-squared (χ^2) (6-7) values of about 33 x 10^{-4} to 98 x 10^{-4}, as shown in Table 1. The interpretation of the physical elements of the proposed equivalent circuit is similar to those previously reported. (4-5-8-11)

Table 1 - Impedance parameters of Pb-3.5 wt.% Sb alloy in 0.5 M H_2SO_4 solution at room temperature.

Parameters	P1	P2	P3
	λ_1 = 30 (±5) μm	λ_1 = 116 (±13) μm	λ_1 = 160 (±20) μm
	λ_3 = N/A	λ_3 = 33 (±8) μm	λ_3 = 47 (±6) μm
R_{el} (Ωcm^2)	4.4	5.1	4.1
$Z_{CPE\ (1)}$ (μFcm^{-2})	411 (± 2.5)	302 (± 5)	802 (± 41)
$Z_{CPE(2)}$(10^{-3}xFcm^{-2})	2.9 (± 0.2)	11.2 (± 4)	0.05 (± 0.01)
n_1	0.79	0.78	0.52
n_2	0.82	0.95	0.98
R_1 (Ωcm^2)	118 (± 4)	320 (± 10)	73 (± 6)
R_2 (Ωcm^2)	215 (± 21)	80 (± 15)	803 (± 35)
χ^2	93 x 10^{-4}	98 x 10^{-4}	33 x 10^{-4}

N/A: Not available

Analyzing the impedance parameters depicted in Table 1, it can be seen that $Z\ (CPE)_{(2)}$ is always lower than $Z(\ CPE)_{(1)}$. Low capacitances can be associated with both an increase in the passive layer thickness (12) and a decrease in the oxide film dielectric constant which is caused by a variation in the ratio of the electrolytic solution volume/oxide film. (12-13-14-15)

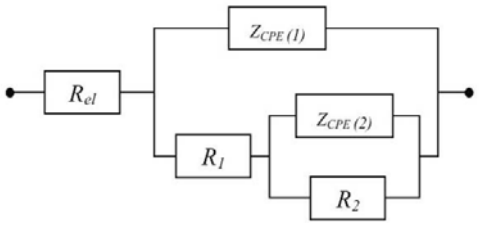

Figure 4 - Proposed equivalent circuit used to obtain impedance parameters.

Comparing the impedance parameters of P1 and P2 samples, it can be observed a reasonable similarity of capacitances $Z\ (CPE)_{(1)}$. On the other hand, P1 has a polarization resistance (R_1) of about 3 times lower than that corresponding to position P2. It seems that the corrosion protection consists of a cooperative action provided by both R_1 and R_2. Thus, the sample P2 has a better electrochemical corrosion behaviour than that of sample P1. When these parameters are compared with those of the sample P3, it can be seen that the sum of R_1 and R_2 attains the highest value of all samples examined, which is associated with the best corrosion resistance. Besides, the highest R_2 value is also that of the sample P3, which can explain that trend to a slope of about 45^o between 0.25 to 0.01 Hz, as shown in Fig. 3. Additionally, it is

important to remark that the capacitance *Z (CPE)$_{(1)}$* corresponds to the capacitance of double layer formation at the surface of the sample, and high *Z (CPE)$_{(1)}$* indicates better electrochemical corrosion response.

b) Potentiodynamic polarization plots

Fig. 5 shows the potentiodynamic polarization curves obtained from -0.75 to -0.35 V (SCE) for the Pb-3.5 wt.% Sb alloy at three (03) different positions (P1, P2 and P3). Parameters and observation of these results reinforce the corrosion resistance trend observed previously with the results of EIS and impedance parameters (equivalent circuit), i.e., better electrochemical corrosion resistance being associated with the sample P3.

Considering the Pb-3.5 wt.% Sb alloy sample at position P1, it is observed a current density of about 16 (±3) µA x cm^{-2} associated with a corrosion potential of about -521 mV (SCE). When similar parameters are observed for samples P2 and P3, the current densities and corrosion potentials are about 10 (±2) µA x cm^{-2} with -520 mV (SCE) and 5 (±2) µA x cm^{-2} with -493 mV (SCE), respectively. It is important to remark that there is no intention to describe the mechanism of dissolution and precipitation of the electrode system, which has been widely discussed by Pavlov et al. (16-17).

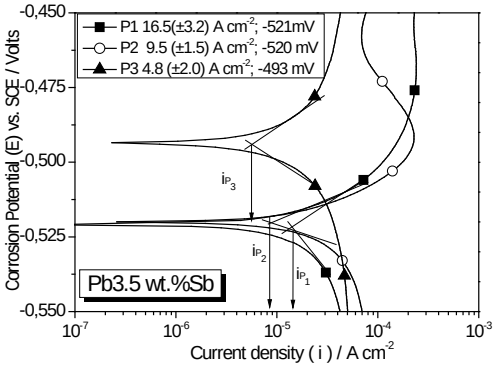

Figure 5 - Potentiodynamic polarization curves exhibiting current densities and corrosion potentials for Pb-3.5 wt.% Sb alloy samples in a 0.5 M H_2SO_4 solution at 25^{o}C, from -0.55 to 0.45 V(SCE).

c) Electrochemical behaviour and resulting microstructures

It is known that during non-equilibrium solidification, the α-phase (Pb-rich) will have an increasingly Sb content from the dendrite arm center toward the interdendritic region up to the eutectic composition. The eutectic mixture is consisted by alternated Pb-rich and Sb-rich phases giving rise to galvanic cells formation.

It was recently reported (4- 7) that a dendritic array has the antimony-rich regions located in the lamellar eutectic mixture. It is also believed that for Pb-Sb dendritic alloys with Sb content higher than 3 wt.%, a finer dendritic array would be more appropriate since it is associated with higher electrochemical corrosion resistance. This is the case of components which are manufactured by continuous casting processes.

Considering the samples examined in this present investigation, it was interesting to observe that with the increase in distance from the bottom of the casting, a trend to decrease the corrosion resistance is clearly confirmed. In order to better understand this apparently contradictory observation when compared with previous studies (4-7) with Pb-Sb alloys having dendritic arrays, the effects of the tertiary dendrite arm spacing associated with antimony macrosegregation for each sample (position) has been evaluated.

These aforementioned assertions permit to explain the reason for which the sample P3 presented a better electrochemical corrosion response than the samples corresponding to the other two examined positions. Firstly, although the position P3 has both coarser primary and tertiary dendritic arms when compared with the corresponding values at P2, its resulting transverse microstructure array has a well defined network of tertiary arms permitting a more homogeneous distribution of the eutectic mixture between the dendritic arms and higher Sb content.

In this context, when the manufacturing of lead-acid battery components is considered, the design of as-cast microstructures can be used as an alternative way to produce as-cast components with different corrosion resistance. In this sense, the choice of cooling rates which will be applied in the manufacturing process in order to attain the best electrochemical response of a Pb-Sb alloy casting should be associated with two initial operational parameters: i) The antimony content of the alloy; and ii) Type of mould. These two parameters will be influent on the resulting cooling rate and microstructure which should be systematically investigated in order to permit the desired electrochemical corrosion response to be attained.

Conclusions

It can be concluded that the tertiary dendritic arm associated with the antimony segregation, which occurs during the casting process, have important roles on the resulting corrosion response. Samples of three transverse sections corresponding to different positions from the bottom of the casting (8, 25 and 50 mm) were examined. It was shown that the sample at position P1 (8 mm) has a dendritic array characterized by only primary (λ_1) and secondary dendrite arm spacings. When comparing the resulting microstructural arrays of positions P3 and P2, it can be seen that the sample at position P3 has tertiary spacings (of about 50 μm) which are coarser than those observed at P2 (λ_3 of about 25 μm) but the continuity of the tertiary arms along the interdendritic region permits the eutectic mixture to be more homogeneously distributed. It can also be concluded that the Sb content and the cooling rate during casting, which determines the magnitude of the dendritic array, are important parameters that should be considered in the manufacture of Pb-Sb alloys components with a view to improving their electrochemical corrosion behaviour.

References

(1) PRENGAMAN, R. D. J. Power Sources, 67 (1997) 267-278.

(2) PRENGAMAN, R.D. in: Proceedings v. 84-14, Advances in Lead-Acid Batteries, BULLOCK, K.R. AND PAVLOV D.; eds., The Electrochemical Society (Pennington, NJ, 1984), p. 201.

(3) REZAEI, B.; DAMIRI, S. J. Solid State Electrochem, 9 (2005), p. 590-594.

(4) OSÓRIO, W.R.; ROSA, D.M.; GARCIA, A. J. Power Sources, 175 (2008), p. 595-603.

(5) OSÓRIO, W.R.; ROSA, D.M.; GARCIA, A. Mater. Des., 34C (2012), p. 660-665.

(6) OSÓRIO W.R.; AOKI, C.; GARCIA, A. J. Power Sources, 185 (2008), p. 1471-1477.

(7) OSÓRIO, W.R.; ROSA, D.M.; PEIXOTO, L.C.; GARCIA, A. J. Power Sources, 196 (2011), p. 6567–6572.

(8) OSÓRIO, W.R.; AOKI, C.S.C.; GARCIA, A. Mater. Sci. Forum 595–598 (2008), p. 851.

(9) PEIXOTO, L.C.; OSÓRIO, W.R.; GARCIA, A. J. Power Sources 195 (2010), p. 621.

(10) SÁ, F.; ROCHA, O.L.; SIQUEIRA, C.A.; GARCIA, A. Mater. Sci. Eng. A, 373 (2004) 131-138

(11) MANSFELD, F.; KENDIG, M.W. J. Electrochem. Soc., 135 (1998), p. 828–835.

(12) GUDIC, S.; RADOSEVIC, J.; KLISKIC, M.: Electrochim. Acta, 47 (2002), p. 3009-3016.

(13) CREMASCO, A.; OSÓRIO, W.R.; FREIRE, C.M.A.; GARCIA, A.; CARAM, R. Electrochim. Acta, 53 (2008), p. 4867-4875.

(14) AZIZ-KERRZO, M.; CONROY, K. G.; FENELON, A. M.; FARRELL, S. T.; BRESLIN, C.B. Biomater., 22 (2001), p. 1531-1539.

(15) OSÓRIO, W.R.; CREMASCO, A.; ANDRADE, P.N.; GARCIA, A.; CARAM, R. Electrochim. Acta, 55 (2010), p. 759-770.

(16) PAVLOV, D.; BOJINOV, M.; LAITINEN, T.; SUNDHOLM, G. Electrochim. Acta, 36 (1991), p. 2081–2086.

(17) PAVLOV, D.; BOJINOV, M.; LAITINEN, T.; SUNDHOLM, G. Electrochim. Acta, 36 (1991), p. 2087–2092.